Supporting Information

Biomimetic Janus Photonic Soft Actuator with Structural Color Self-Reporting

Yong Qi,[a] Changtong Zhou,[a] Yisong Qiu,[b] Xianfei Cao,[a] Wenbin Niu,[a] Suli Wu,[a] Yonggang Zheng,[b] Wei Ma,[a] Hongfei Ye,[b] and Shufen Zhang[a]*

[a] State Key Laboratory of Fine Chemicals, Dalian University of Technology, P.O. Box 89, West Campus, 2# Linggong Rd, Dalian 116024, China

[b] International Research Center for Computational Mechanics, State Key Laboratory of Structural Analysis for Industrial Equipment, Department of Engineering Mechanics, Faculty of Vehicle Engineering and Mechanics, Dalian University of Technology, Dalian 116024, China

*E-mail: zhangshf@dlut.edu.cn

Experimental Section

Materials. Ethoxylated trimethylolpropane triacrylate (ETPTA), polyethylene glycol (200) diacrylate (PEGDA), ethylene glycol methyl ether acrylate (MEA), superfine spherical copper powder, and n-hexadecyl mercaptan were purchased from Aladdin. Hydrofluoric acid (HF, 40 wt %), sodium hydroxide (NaOH), and ammonium persulfate ($(NH_4)_2S_2O_8$) and were purchased from Fuyu Chemical Reagent Factory. Butyl methacrylate (BMA, Tianjin Damao Chemical Reagent Factory), dichloromethane (as the oil phase, Tianjin Damao Chemical Reagent Factory), chloroform (Tianjin Damao Chemical Reagent Factory), ethyl acetate (Tianjin Damao Chemical Reagent Factory), toluene (Beijing Chemical Works), and n-hexane (Tianjin Fuyu Fine Chemical Co., Ltd.) were used as received.

Preparation of the JPSA. SiO_2 nanospheres were prepared as our reported method.[1] SiO_2 (~285 nm) photonic crystal "Template B" was prepared via the dip-coating method. The ultrafine spherical copper powder was deposited on a plexiglass plate to obtain "Template A". Patterned "Template A" can be used to prepare the JPSA for shape conversion. Combining "Template A" with "Template B" to form a "sandwich" template, where the gaps between two layers were separated by polyimide tape. By utilizing capillary force, the interstitials in-between SiO_2/copper microspheres of the "sandwich" template were filled up with oligomer mixtures consisting of ETPTA, PEGDA (200), and BMA with volumetric ratio 1:5:2.5. Darocur 1173 (2-hydroxy-2-methyl-1-phenyl-1-propanone, BASF, 1 wt %) was added as photoinitiator. The "sandwich" template was photopolymerized by using a pulsed UV curing system (RC 742, Xenon) for 2 min. The solidified film was soaked in a 5 vol % HF aqueous solution for 2 min and finally rinsed with deionized water. The bilayer film was immersed in a mixed solution (100 mL) of NaOH (5 g) and $(NH_4)_2S_2O_8$ (1.5 g) for 30 min.[2] Then the obtained bilayer film was immersed in a mixed solution of n-hexadecyl mercaptan and ethanol for 12 h after washing with deionized water and ethanol. The target JPSA can be obtained by connecting the "Layer A" and "Layer B" through a mechanical-drilled channel. The monomer ratio adopted by the rapid responsive JPSA is ETPTA/MEA/BMA=1:5:2.5.

Characterization. A scanning electron microscope (Nova Nano SEM 450; Testing Conditions: HV, 10 kV; Spot, 3.0) was used to characterize the morphology of the SiO_2 nanospheres and inverse opals. The retroreflectance and the reflectance spectrum of the JPSA were recorded by a spectrophotometer (Hitachi U-4100, Japan) and a Fiber Optic Spectrometer (EQ 2000). The optical microscope (Autor optics MIT series metallographic microscope, Testing Conditions: objective lens, ×80; ocular lens, ×10) was used to observe the swelling process of the "Layer A". Advanced Fourier Transform infrared Spectrometer (Thermo Fisher 6700, KBr pellet) was used to analyze the polymer. The adhesion mechanics were measured by Contact Angle Meter and Tensiometer (Krüss K100, Germany). The apparent water and the oil contact angles were measured by using a JC2000D1 contact-angle system (Powereach, China). Huawei honors V20 was used to capture all the photographs of

the samples. The tensile strength test was conducted with PT-305 Computer universe testing machine from Dongguan Precise-test Equipment Co., Ltd. A homemade device was used for the bending test and the minimum distance between the clamps was 5 mm.

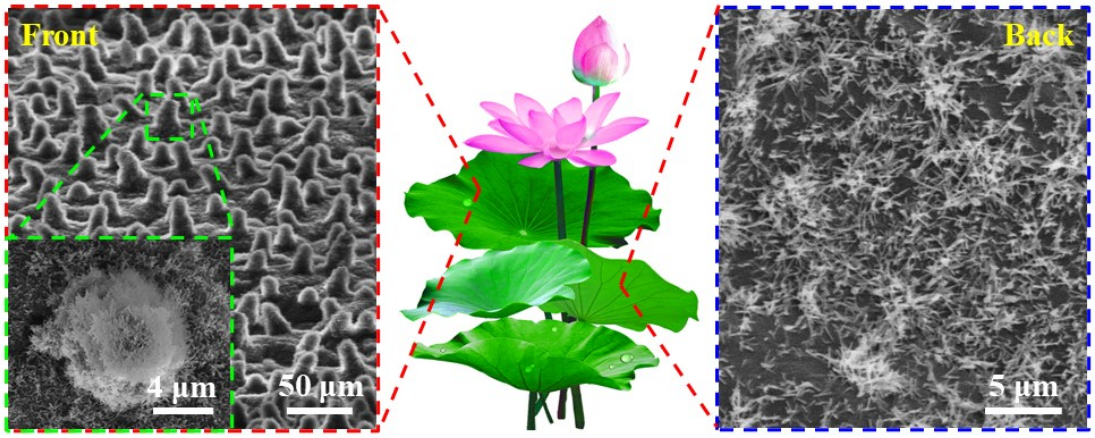

Figure S1. The micro-nano structures of the front/back of lotus leaf. These micro-nano structures make the front side superhydrophobic, while the back side is hydrophilic.[3]

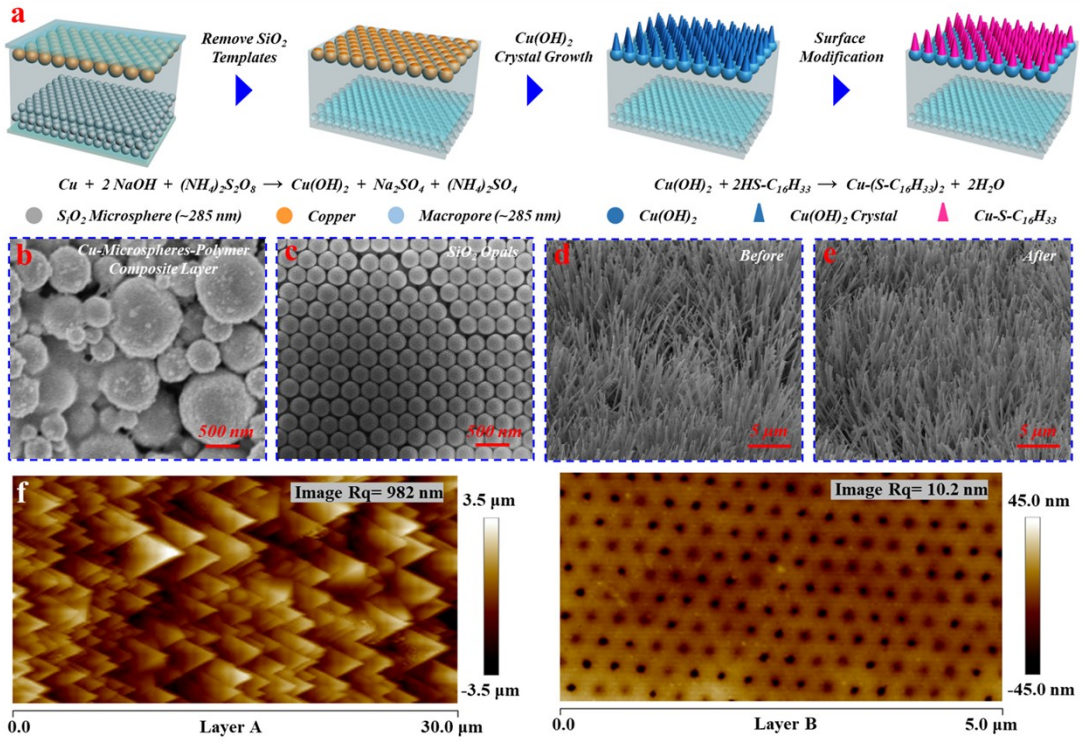

Figure S2 (a) Schematic of the fabrication of the JPSA; (b) Typical SEM image of the "Layer A" of the ultrafine spherical copper composite film before modification; (c) Typical SEM image of silica opal in "Layer B". The composite bilayer film was obtained by combining "Template A" (ultrafine spherical copper powder, 0.2-1 μm) and "Template B" (silica opal, diameter of ~285 nm) and photopolymerizing after

filling acrylate monomer. The reverse opal film with a micro-nano copper array on the back was obtained by etching silica with 5 % hydrofluoric acid; Typical SEM images of the "Layer A" before (d) and after (e) hydrophobic modification; (f) Typical atomic force microscope (AFM) images of"Layer A" and"Layer B". The roughness values of the"Layer A" and"Layer B" are ~982 nm and ~10.2 nm, respectively. The size difference of micro/nano arrays in AFM and SEM images can be attributed to the growth of copper arrays.

The underwater super-oleophilic "Layer A" was prepared by soaking in a mixed solution of n-hexadecyl mercaptan and ethanol for 24 h after etching the copper micro-nano array in a mixed solution of NaOH and $(NH_4)_2S_2O_8$.[2] Acicular $Cu(OH)_2$ micro-nano crystals grew out from the copper-polymer composite surface in this procedure. The surface morphologies of the "Layer A" show no remarkable differences before and after the surface modification.

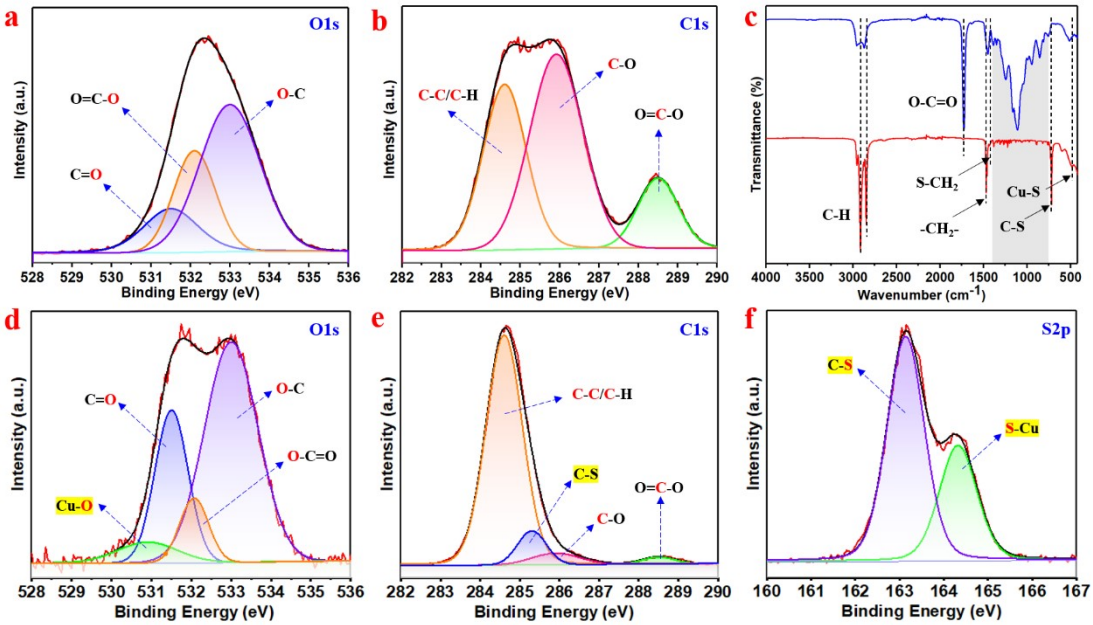

Figure S3. The XPS spectra of the "Layer A" before preparing copper hydroxide crystals, (a) O1s; (b) C1s; (c) FT-IR spectra of the "Layer A", the blue curve is obtained under the transmission mode and the red curve is obtained under the reflection mode; The XPS spectra of the "Layer A" after hydrophobic modification, (d) O1s; (e) C1s; (f) S2p.

The binding energy positions obtained by O1s peaking are 531.5, 532.1, and 533 eV, corresponding to the C=O, O-C=O, and O-C bonds, respectively. A new peak of 530.9 eV was produced after the modification of mercaptan, which could be attributed to the Cu-O bond.[4, 5] The binding energy positions obtained by C1s peaking are 284.6, 285.9, and 288.5 eV, corresponds to the C-C/C-H, C-O, and O=C-O bond, respectively. A new peak of 285.3 eV was produced after the modification of mercaptan, which could be attributed to the C-S bond.[6] The binding energy positions obtained by S2p peaking are 163.1 and 164.3 eV, corresponding to the S-C and S-Cu bond, respectively.[7]

The C-H stretching vibration absorption peaks appear at 2960-2840 cm^{-1}. The C=O stretching vibration absorption peaks appear at ~1730 cm^{-1}. The CH_2 deformation vibration absorption peaks appear at ~1470 cm^{-1}. The C-S stretching vibration absorption peaks appear at ~720 cm^{-1}. The S-Cu stretching vibration absorption peaks appear at ~486 cm^{-1}. The CH_3 deformation vibration absorption peaks appear at ~1393 and 1350 cm^{-1}. The C-O stretching vibration absorption peaks appear at ~1257 cm^{-1}. The C-O-C stretching vibration absorption peaks appear at ~1170 and ~1100 cm^{-1}. The weak absorption peaks between 1450 and 700 cm^{-1} under the reflection mode might be attributed to a large amount of n-hexadecyl mercaptan covering the polymer chain after modification.

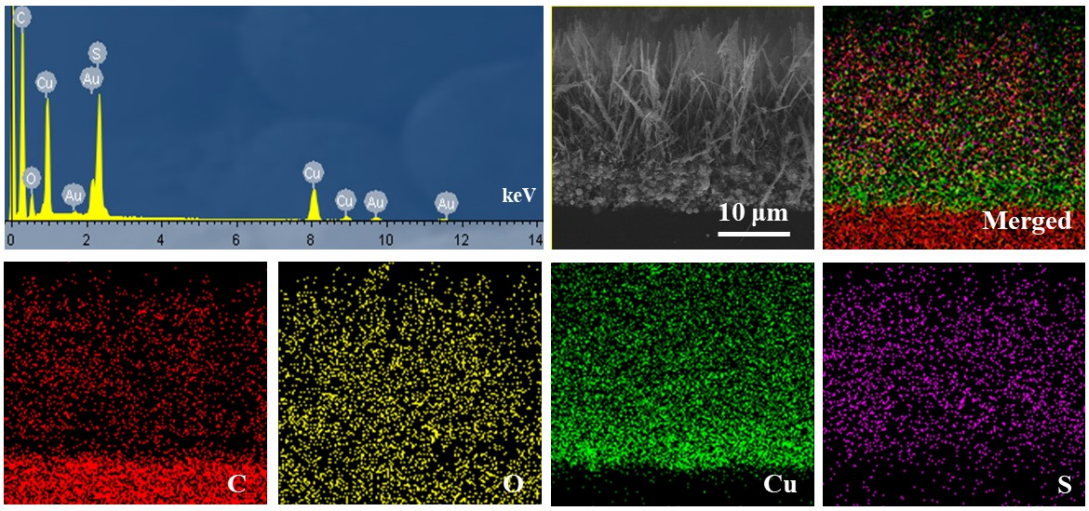

Figure S4. Typical energy-dispersive X-ray spectroscopy (EDS) analysis, cross-sectional SEM image, and the EDS mapping images of C (red), O (yellow), Cu (green), and S (purple) of the "Layer A" after hydrophobic modification. The distribution diagram of elements further illustrates the reliability of surface modification.

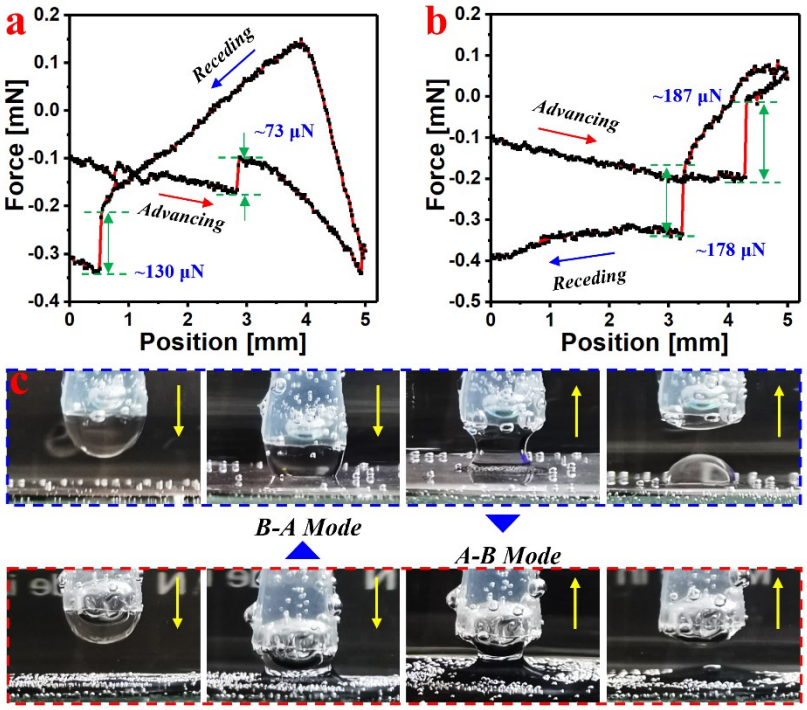

Figure S5. The adhesion of underwater oil droplets on both surfaces of the JPSA, (a) B-A Mode, (b) A-B Mode; (c) Typical digital photos of the adhesion process in a-b. The wetting force of underwater oil droplets on the surface of "Layer B" (~73 μN) is less than that of "Layer A" (~187 μN). The adhesion force during the receding process on "Layer A" (~178 μN) is greater than that of "Layer B" (~130 μN).

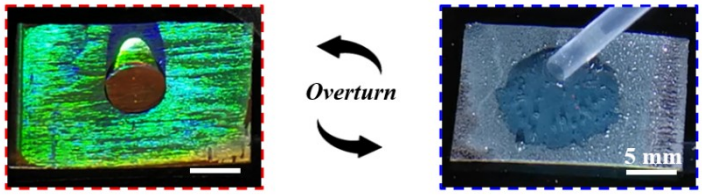

Figure S6. The contact state of oil droplets on both sides of the JPSA. In B-A Mode, the oil droplets appear to be aggregated, while in A-B Mode, they appear to be dispersed. The incident and observation angles are ~60 ° and ~50 °, respectively. "Layer A" is more conducive to the diffusion of underwater oil.

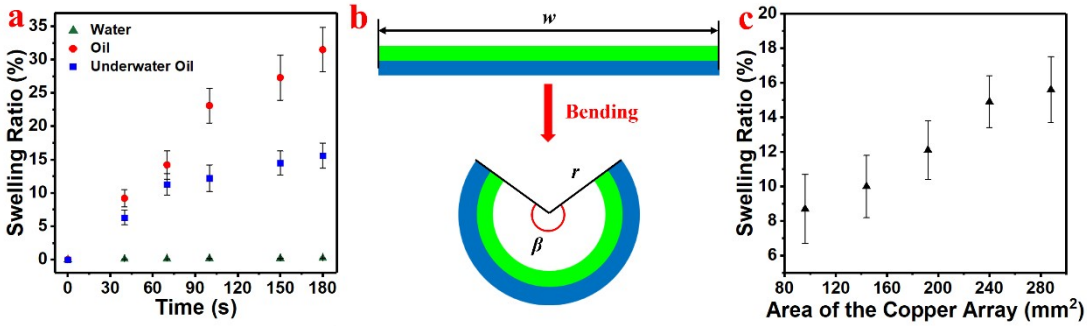

Figure S7. (a) The swelling rate of the Janus film varies with time; (b) Schematic illustration of the bending process of the Janus film; (c) Relationship between

swelling rate and the area of the copper array. The size of the film is 24×12 mm, the swelling time is 180 s, the area of the copper array can be controlled by adjusting the area of the deposited copper powder.

The source of the actuation was the difference of oil-absorption-induced swelling between the "Layer A" and "Layer B". Due to the super-hydrophobicity of "Layer A" and the weak hydrophilicity of "Layer B", the swelling rate of Janus film in the water phase is almost constant. In the oil phase, the super-lipophilicity of the polymer causes the swelling of the Janus film. However, the Janus film does not bend due to the swelling difference between "Layer A" and "Layer B" is almost zero. Interestingly, in the water-oil system (the "Layer A" is in contact with the oil phase and the "Layer B" is in contact with the water phase), the difference of the underwater oil wettability of "Layer A" and "Layer B" leads to the difference in oil-absorption-induced swelling, showing directional actuating. The swelling ratio that measures the extent to which a Janus film absorbs water/oil is defined as follows: $\eta=(w_t-w_0)/w_0\times100\%$,[8] where w_0 and w_t are the weights of the films before and after immersing in water, oil, or water-oil mixture. The curvature (κ) during the underwater oil-induced actuating was calculated according to the following equations: $\kappa=(\beta\pi)/(180w)$,[9] where w is the length of the actuator along the bending direction, β is the bending angle of the bending arch (Figure S7b).

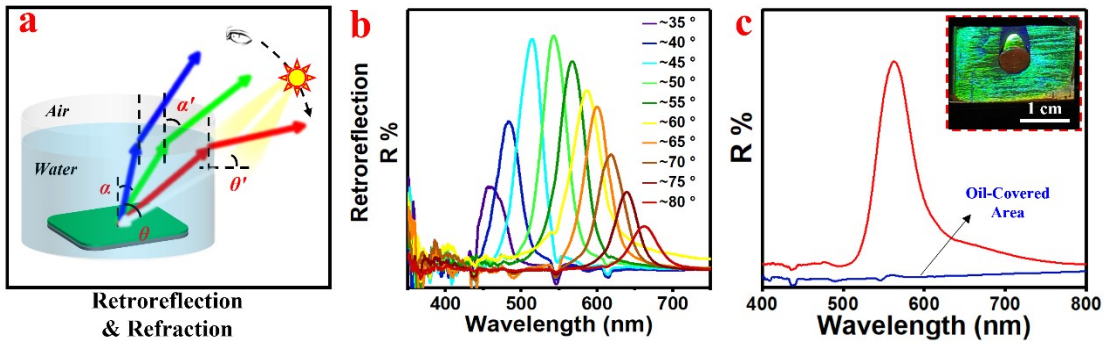

Figure S8. (a) Retroreflection diagram of "Layer B"; (b) Retroreflection spectrum of the JPSA in Figure 2d, the incident angle is ~60 °, the detection angle changes from ~35 ° to ~80 °; (c) The retroreflection of "Layer B" in water shows strong diffraction light, however, the diffraction light disappears in the oil-covered area. The incident and observation angles are ~60 ° and ~50 °, respectively.

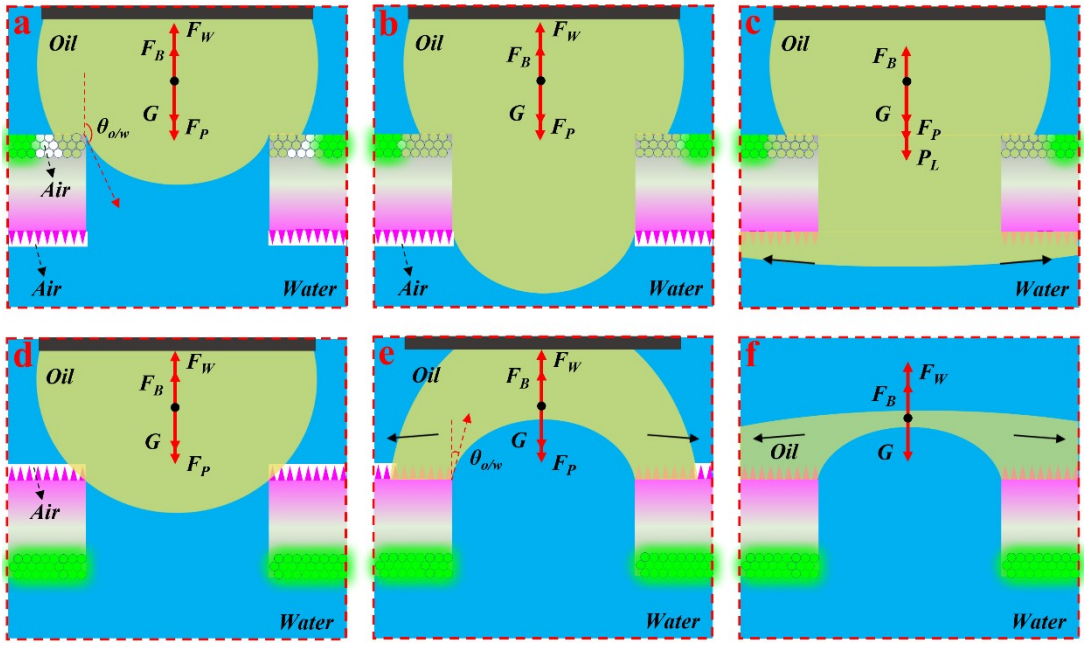

Figure S9. Possible force analysis of unidirectional permeation of underwater oil droplets, (a-c) B-A Mode, (d-f) A-B Mode. Since the UOCA is greater than 90 ° (B-A Mode, non-wetting), the direction of wetting resistance force (F_W) in the channel is upward (the same as buoyancy, F_B), which hinders the downward transport of oil droplets. Gravity (G) and the pump (F_P) force the oil droplets to continue passing through the channel in the polymer. In case of the oil touches the superhydrophobic (super-oleophilic) "Layer A", it spreads out rapidly. This generates an oil channel (so-called Laplace channel) between the oil and under-gas layer in "Layer A". Once the channel forms, a differential Laplace pressure (P_L) is generated in the oil phase. Moreover, the F_W disappears as the channel is filled with oil. In A-B Mode, however, there is no P_L between the oil and "Layer B" due to the dominant role of diffusion.

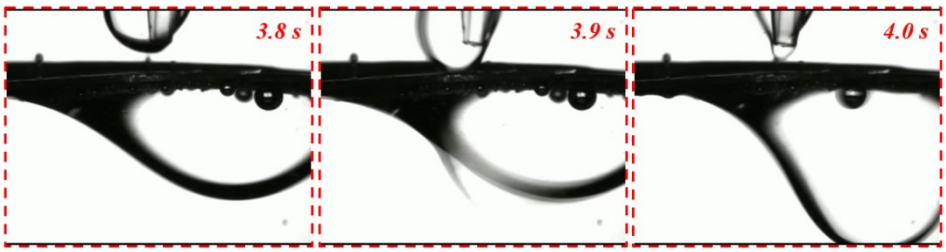

Figure S10. Oil pass through the Janus film based on the oil-"Layer A" channel. Once the P_L is formed, the F_W disappears as the channel is filled with oil. Continuous drops of oil pass through the channel quickly due to the reduction of the resistance.

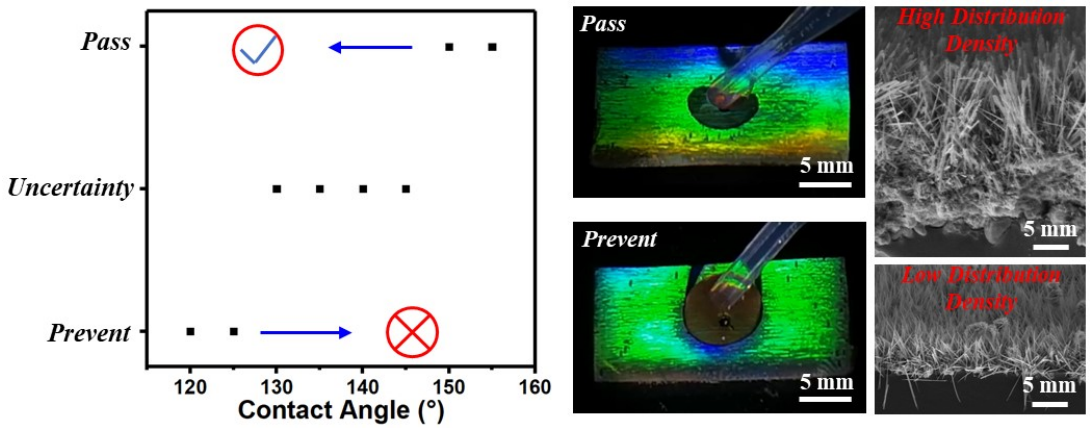

Figure S11. The effect of the hydrophobicity of"Layer A" on the unidirectional permeability of underwater oil droplets. The middle insets are the corresponding photos of JPSA, the right insets are the corresponding SEM images of "Layer A". When WCA is greater than 150 ° (superhydrophobic, prepared by using copper powder with high distribution density), oil droplets can easily pass through the channel. However, it is difficult to pass through the channel when WCA is less than 125 ° (hydrophobic, prepared by using copper powder with low distribution density). The hydrophobicity of "Layer A" can be controlled by increasing the distribution density of copper powder. The greater the distribution density of the copper powder is, the higher the copper micro-nano array is, thus the thicker the air layer retained by the prepared superhydrophobic copper micro-nano array in water. Superhydrophobicity of the "Layer A" facilitates the diffusion of underwater oil droplets. The air layer contributes to the formation of the Laplace channel.

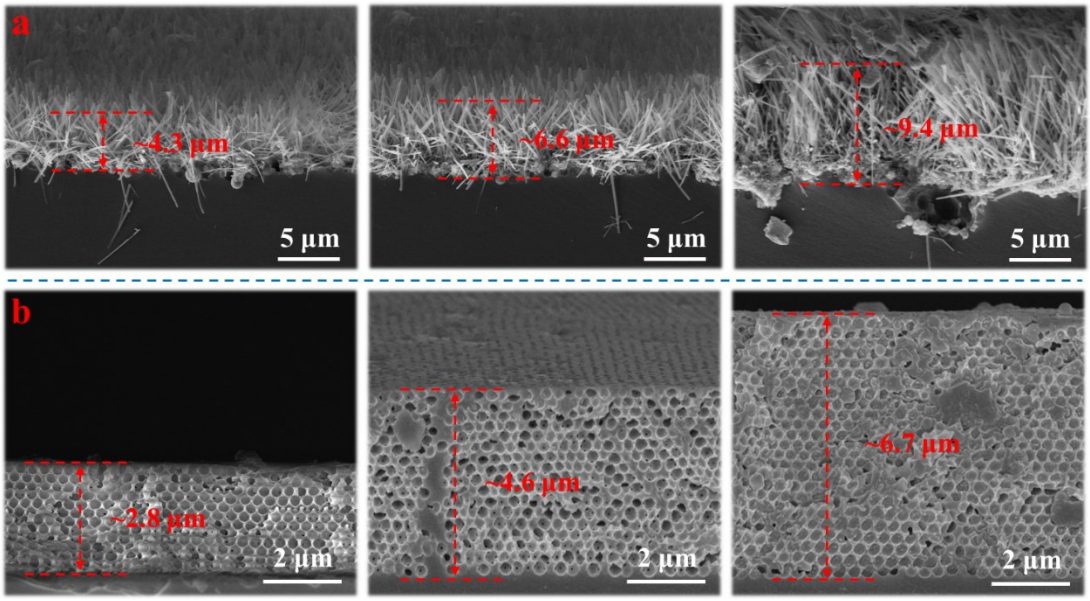

Figure S12. SEM images of (a) "Layer A" and (b) "Layer B" with different thicknesses. The thickness of "Layer A" can be regulated by using copper powder with different distribution densities. The greater the distribution density of the copper powder is, the greater the thickness of the copper array is. The thickness of "Layer B" can be regulated by using SiO_2 opals with different thicknesses.

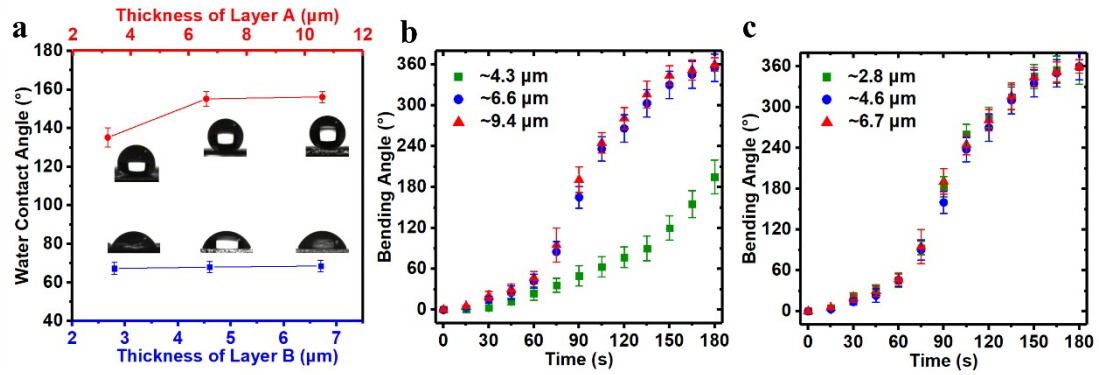

Figure S13. (a) WCAs on "Layer A" and "Layer B" with different thicknesses; (b) Bending tests of JPSA constructed by "Layer A" with different thicknesses and "Layer B" with a fixed thickness (~4.6 μm); (c) Bending tests of JPSA constructed by "Layer B" with different thicknesses and "Layer A" with a fixed thickness (~9.4 μm).

Because the composite film is insensitive to water but sensitive to oil, the source of the actuation was the difference of oil-absorption-induced swelling between the "Layer A" and "Layer B". Superhydrophobicity of the "Layer A" facilitates the diffusion of underwater oil droplets. The bending rate increases with the increase of the thickness of "Layer A". The underwater oleophobicity of "Layer B" is not conducive to the diffusion of underwater oil droplets. The thickness of "Layer B" has little effect on the bending rate. It might be attributed to the underwater super-oleophilic of "Layer A" and the underwater oleophobic of "Layer B". The thicker the "Layer A", the thicker the air layer locked in the superhydrophobic copper array in water, the more conducive to the diffusion of oil droplets on the surface. The air layer contributes to the formation of the Laplace channel, while the thickness of the "Layer B" has little influence on the formation of the Laplace channel due to the invariable wettability. However, when the WCA exceeds 150 °, the thickness has little influence on the actuation rate. It might be attributed to the similar diffusion rates of underwater oil droplets on the two superhydrophobic surfaces.

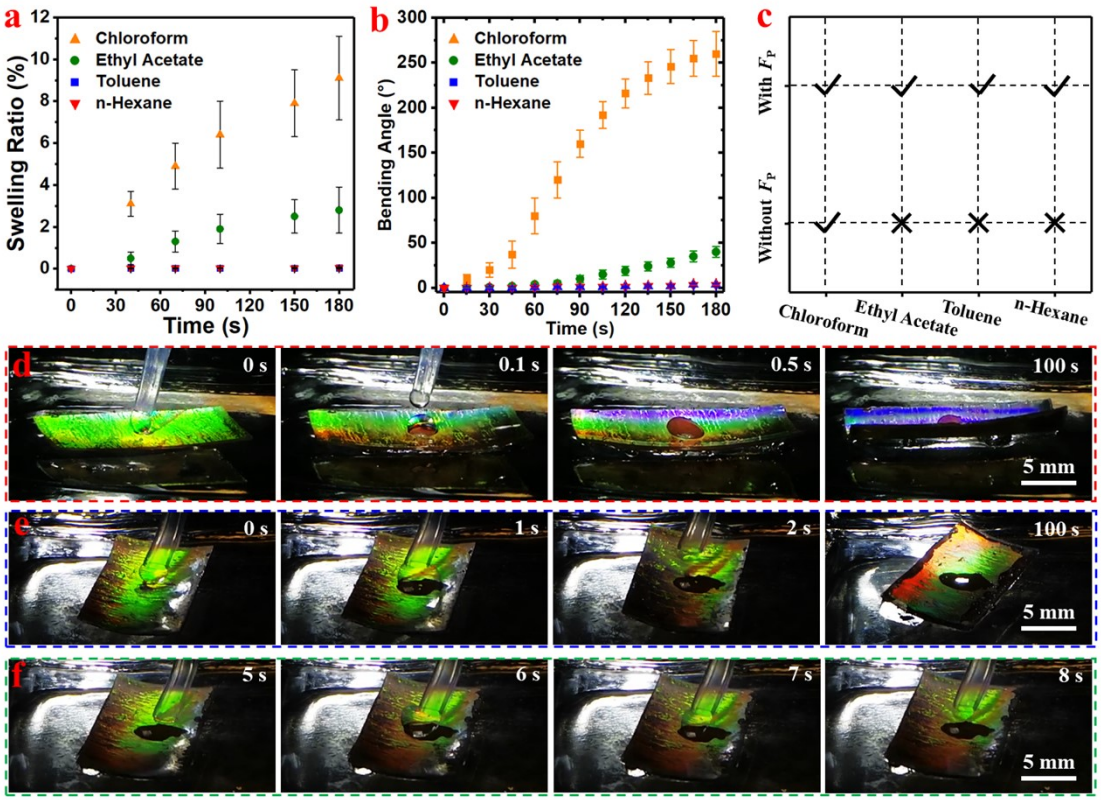

Figure S14. (a) The swelling rate of the Janus film ("B-A Mode") in oil (including chloroform, ethyl acetate, toluene, and n-hexane)-water solutions varies with time; (b) The effect of the types of oil on the bending of JPSA ("B-A Mode"); (c) The effect of the types of oil on the unidirectional permeability of underwater oil droplet ("B-A Mode"). Chloroform (density, 1.484 g/mL) can pass through the channel without pressure, while the ethyl acetate (density, 0.902 g/mL), toluene (density, 0.866 g/mL), and n-hexane (density, 0.692 g/mL) could pass through the channel only under applied pressure. It might be attributed to the balance between G, P_L, F_B, and F_W; Typical bending process and corresponding structural colors induced by (d) chloroform and (e) n-hexane, the initial incident and observation angles are ~60 ° and ~50 °, respectively ("B-A Mode"); (f) n-Hexane pass through the Janus film based on the oil-"Layer A" channel. In "B-A Mode", the P_L, F_P, and G collectively overcome the F_B and F_W, so the oil is transported instead of resting on the oil-phobic "Layer B". Once the P_L is formed, the F_W disappears as the channel is filled with oil. Continuous drops of oil pass through the channel quickly due to the reduction of the resistance.

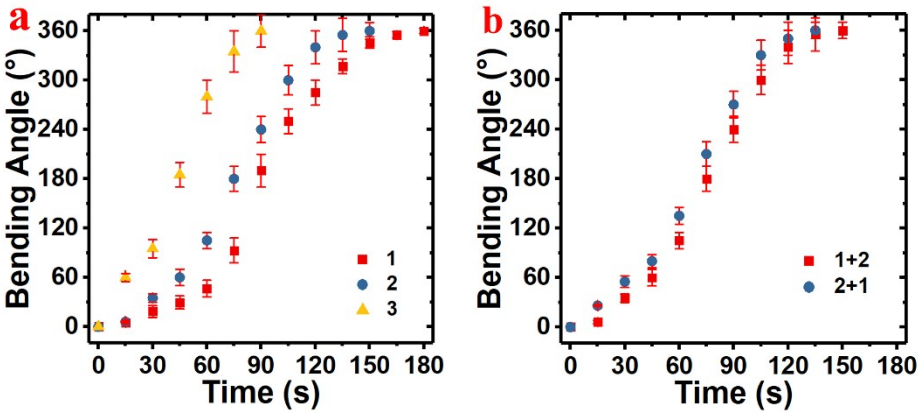

Figure S15. (a) The effect of the number of oil drops (1-3 drops) on the bending of JPSA in Figure 4b. The more oil droplets, the faster the swelling rate of "Layer A", and the shorter the time for a 360 ° bending; (b) The effect of the number of channels (1 and 2 holes) on the bending of JPSA in Figure 4b. "1+2" means adding two drops of oil to one channel (only one hole), and "2+1" means adding one drop of oil to each channel (two holes in total).

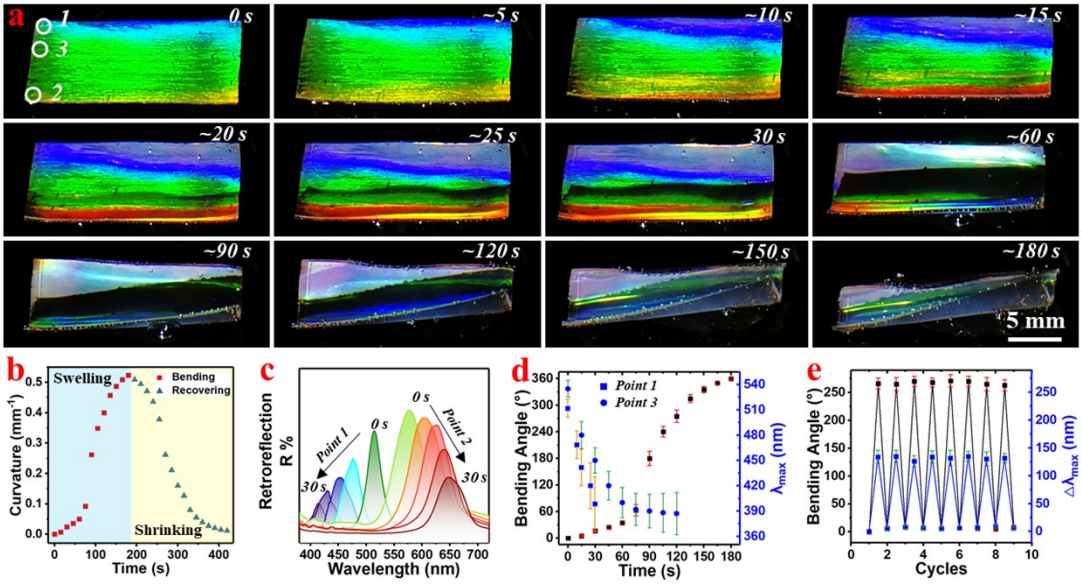

Figure S16. (a) Typical swelling process and corresponding structural colors, the initial incident and observation angles are ~60 ° and ~50 °, respectively (Without channel, the oil is injected from the bottom, points 1, 2, and 3 were used for spectroscopic determination). As the curvature increases, the edge 1 shifts from green/cyan to purple, while the edge 2 shifts from green to red. When the Janus film swells unevenly from left to right, it also leads to a change of structural color in the transverse direction (from red to blue); (b) Curvature changes of the Janus film during bending and recovering (drying at ~50 ℃) processes; (c) The retroreflection spectrum of the point 1 and 2 in (a); (d) The maximum peak of the retroreflection (λ_{max}) of point 1 & 3 and the bending angles of the Janus film in (a); (e) The bending cycles of the Janus film. The bending angles are the central angles corresponding to ~120 s. The

maximum reflection shifts ($\Delta\lambda_{max}$) are the displacement values of the reflection peaks corresponding to endpoint 3 at 120 s.

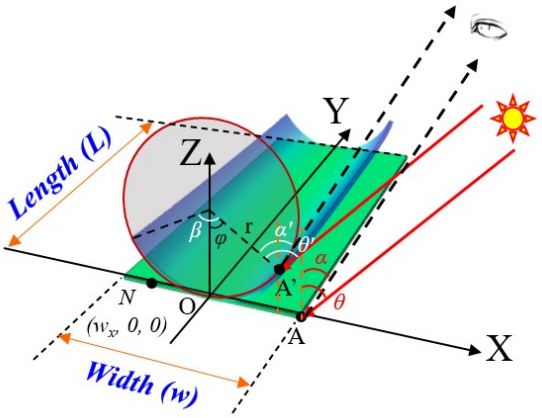

Figure S17. Schematic diagram of measurement of corresponding parameters during the bending process. The Janus film is 24 mm in length, 12 mm in width, and 0.3 mm in thickness. r is the radius of the inner tangent circle of the bending surface. The variation of structural color is caused by the bending-induced change of θ and α.

The relationship between curvature (κ=1/r) and bending angle (β) could be considered as:

$$\kappa=(\pi\beta)/(180w) \qquad (1)$$

The central angle (φ) corresponding to arc OA' can be calculated as:

$$\varphi=\beta/2 \qquad (2)$$

The increment of the incident ($\Delta\theta$) and observation ($\Delta\alpha$) angles can be approximated as:

$$\Delta\theta \approx \theta' - \theta = \varphi \qquad (3)$$

$$\Delta\alpha \approx \alpha' - \alpha = \varphi \qquad (4)$$

According to the equation (1-4), the changes of bending angle, curvature, incident angle, and observation angle of the JPSA during the bending process could be approximated. According to the symmetric relation, the incident and observation angles of the negative X-axis show a decreasing trend, and the decreasing size is positively correlated with φ. The Z-axis shift of endpoint I causes the corresponding incident and observation angles to decrease, while endpoint II increases. When the initial incident angle is ~60 °, the redshifted structural color can be observed at the endpoint II in the interval $0 \leq \beta < 60$ °. This is roughly consistent with the experimental results.

Setting the coordinate of point N on the initial boundary as (w_x, *0, 0*). According to formula (1-2), the central angle (φ_x) corresponding to the arc OX formed by this point during the bending process can be calculated as:

$$\varphi_x = (w_x\beta)/(2w) \qquad (5)$$

Retroreflection at point N mainly depends on the change of bending angle and the length (x-coordinate, w_x) from the central axis. This means that the closer to the Y-axis, the longer the time for the structural color to be observed. The reason could be considered as the incident light will be blocked by "Layer A" when θ' exceeds 90 °.

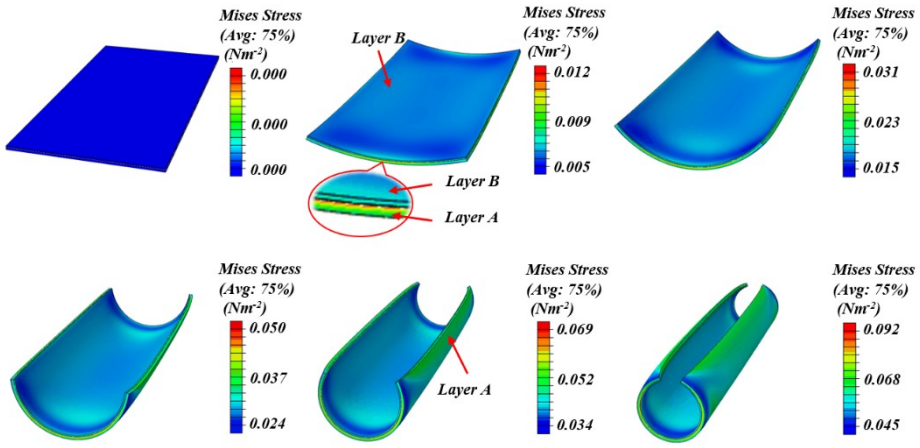

Figure S18. Finite element simulation of stress distribution of Janus film during bending process (B-A Mode, Without Channel). During the initial stage of swelling, the stress concentrates on the edge of "Layer A". The stress of the non-swelling "Layer B" mainly comes from the extrusion and distortion of the bending of "Layer A", which is less than the internal stress of "Layer A". Inner-stress transfer (from the edge to the whole surface) exists during the bending process.

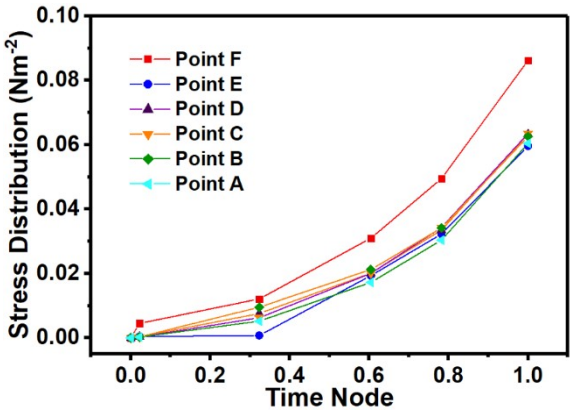

Figure S19. The stress distribution of points A-F in Figure 4c. The stress distribution intensity increases with the increase of time nodes.

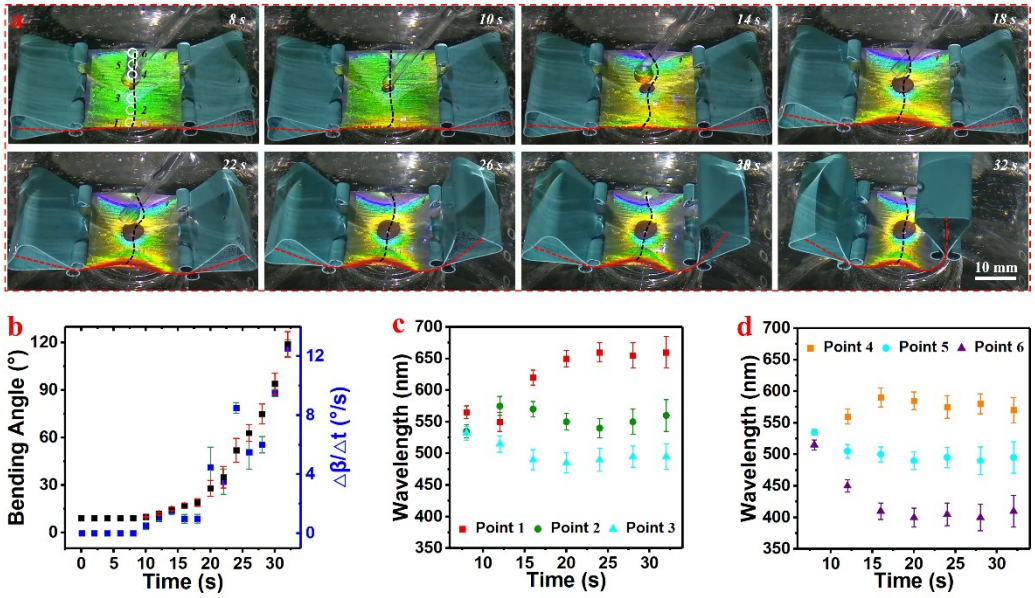

Figure S20. (a) Load lifting processes of the JPSA triggered by UOUP (channel diameter is ~1 mm, the incident angle is ~60 °, the observation angle is ~50 °); (b) The relationship between bending angle/bending rate ($\Delta\beta/\Delta t$) and time in (a); (c) The retroreflection spectrum of the point 1, 2, and 3 in (a); (d) The retroreflection spectrum of the point 4, 5, and 6 in (a).

In B-A Mode, the JPSA can easily lift two heavy objects (a total of 40 times the weight of the JPSA), while the changing structural color can track the swelling of the film. According to the previous experimental results, the stress distribution and transfer during the actuating process can be easily analyzed in combination with the change of structural color. We tracked the structural colors of six areas along the central axis. The redder (or purpler) the color, the greater the strain and stress. At the initial stage of swelling, the change bending angle of JPSA is slow, but once the weight is lifted, the rate increases exponentially. This might be related to the change in the swelling rate.

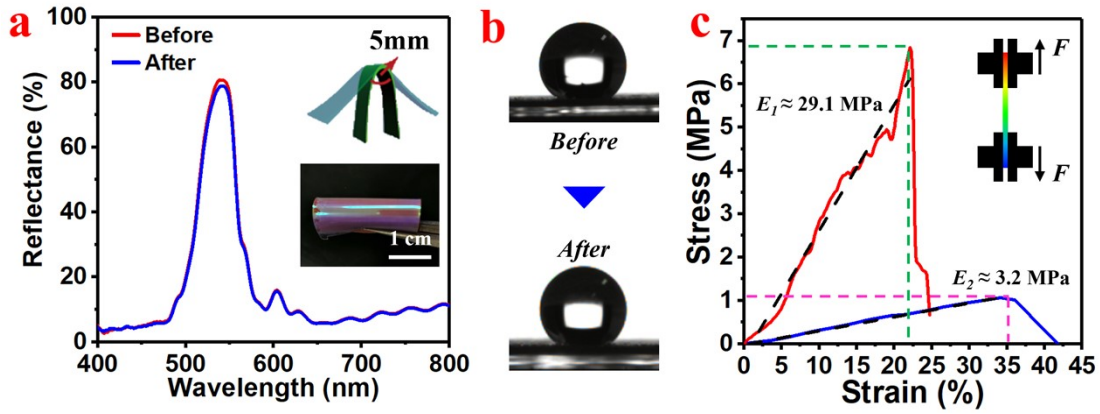

Figure S21. (a) Specular reflection of "Layer B" (the Janus film prepared by using ETPTA, PEGDA (200), and BMA) before and after 100 bending cycles. The insets are the diagram of the bending test and the corresponding digital photo; (b) The WCA of "Layer A" before and after 100 bending cycles; After 100 bending experiments, the

specular reflectance of “Layer B” and the WCA of “Layer A” show almost no reduction, which further proves its practicability; (c) Tensile strain curves of the JPSA (red curve) and the rapid responsive JPSA (blue curve). The black dotted line is a linear fit of the corresponding curve. At the stage of elastic deformation, the stress and strain become directly proportional (that is, in accordance with Hooke's Law), and its proportional coefficient is the so-called elastic modulus (*E*). The elastic modulus of the JPSA is ~29.1 MPa, while the elastic modulus of the rapid responsive JPSA is ~3.2 MPa. According to Figures 4d and 5g, a lower *E* is conducive to improving the sensitivity of the Janus film.

Video 1. Permeation of underwater oil on JPSA (B-A Mode, the channel diameter is ~1 mm).
Video 2. Permeation of underwater oil on JPSA (B-A Mode, the channel diameter is ~1 mm, the incident angle is ~60 °, the observation angle is ~50 °).
Video 3. The spreading of underwater oil on JPSA (A-B Mode, the channel diameter is ~1 mm).
Video 4. The spreading of underwater oil on JPSA (A-B Mode, the channel diameter is ~1 mm, the incident angle is ~60 °, the observation angle is ~50 °).
Video 5. The spreading of the oil-water interface on “Layer A” after penetrating the channel (B-A Mode, the WCA of “Layer A” is ~136 °).
Video 6. The actuating process of JPSA triggered by UOUP (B-A Mode, the incident angle is ~60 °, the observation angle is ~50 °, Speed×3).
Video 7. The actuating process of the fast responsive JPSA triggered by UOUP (B-A Mode, the incident angle is ~60 °, the observation angle is ~50 °, Speed×1).

References

1 Y. Qi, W. Niu, S. Zhang, S. Wu, L. Chu, W. Ma, B. Tang, *Adv. Funct. Mater.* 2019, **29**, 1906799.
2 C. Pei, Y. Peng, Y. Zhang, D. Tian, K. Liu, L. Jiang, *ACS Nano* 2018, **12**, 5489-5494.
3 C. Zhang, Y. Zhang, X. Xiao, G. Liu, Z. Xu, B. Wang, C. Yu, R.H.A. Ras, L. Jiang, *Green Chem.* 2019, **21**, 6579-6584.
4 Z.-Y. Luo, K.-X. Chen, J.-H. Wang, D.-C. Mo, S.-S. Lyu, *J. Mater. Chem. A* 2016, **4**, 10566-10574.
5 C.H. Kung, B. Zahiri, P.K. Sow, W. Mérida, *Appl. Surf. Sci.* 2018, **444**, 15-27.
6 W. Zhou, G. Li, L. Wang, Z. Chen, Y. Lin, *Appl. Surf. Sci.* 2017, **413**, 140-148.
7 M. Khosravi, S. Azizian, R. Boukherroub, *Sep. Purif. Technol.* 2019, **215**, 573-581.
8 X. Su, H. Li, X. Lai, Z. Chen, X. Zeng, *Chem. Eng. J.* 2020, **394**, 124919.
9 Z. Zhang, Y. Qi, W. Ma, S. Zhang, *ACS Appl. Mater. Interfaces* 2021, **13**, 2007-2017.